J. Fluid Mech. (1989), *vol.* 202, *pp.* 149–176
Printed in Great Britain

Rossby–Kelvin instability: a new type of ageostrophic instability caused by a resonance between Rossby waves and gravity waves

By SATOSHI SAKAI

Department of Earth Science, College of Liberal Arts, Kyoto University, Kyoto 606, Japan

(Received 19 October 1987 and in revised form 21 July 1988)

An ageostrophic version of Phillips' model is studied. All instabilities found are systematically interpreted in terms of resonance of wave components. The instability occurs if there is a pair of wave components which propagate in the opposite direction to the basic flow and these wave components have almost the same Doppler-shifted frequency. A new instability, identified as a resonance between the Kelvin wave and the Rossby waves, is found at Froude number $F \approx 0.7$. The Rossby waves are almost completely in geostrophic balance while the ageostrophic Kelvin wave is the same as in a one-layer system. Doppler shifting matches frequencies which would otherwise be very different. This instability is presumably the mechanism of the frontal instability observed by Griffiths & Linden (1982) in a laboratory experiment. Ageostrophic, baroclinic instability with non-zero phase speed is also observed in the numerical calculation. This instability is caused by resonance between different geostrophic modes.

1. Introduction

Since the pioneering works of Charney (1947) and Eady (1949), baroclinic instability has been of interest in geophysical fluid dynamics and studied by many researchers theoretically and experimentally (Hide & Mason 1975). The mechanism of this instability is most simply illustrated by Phillips' two-layer model (Phillips 1954). In the model, baroclinic instability occurs when two layers have opposite gradients of potential vorticity (Pedlosky 1979). Because the timescale of this phenomenon is usually very long, most of these studies were done in a framework of low-frequency quasi-geostrophic dynamics in which gravity waves are excluded *a priori*.

Kelvin–Helmholtz instability has also been well known since the work of Kelvin (1871). For this instability, gravity waves are essential. Therefore it has been studied mainly in a non-rotating frame. Although these two instabilities may occur in the same configuration (for example, a two-layer model with basic shear and rotation), they have been discussed in different contexts and never considered together, except by Orlanski (1968).

Recently, Ripa (1983) generalized the stability criterion for the quasi-geostrophic model (essentially the Rayleigh–Fjortoft theorem) to shallow-water equations. This criterion is interpreted more intuitively by Hayashi & Young (1987): instability occurs when a wave having positive disturbance momentum resonates with another wave having negative disturbance momentum. The resulting unstable mode has zero disturbance momentum. This is not a sufficient condition for instability, but is still

a very useful criterion because once we know the dispersion curve and disturbance momentum for waves, we can often predict where instability will occur. Although their model was a one-layer model, this result can be extended to a two-layer model.

A most important point is that this criterion does not restrict the wave type that may cause resonance. Therefore, we can expect an instability with new combinations: Rossby waves and gravity waves. (Throughout this paper, waves related to a gradient of the basic potential vorticity are called Rossby waves. Therefore 'Rossby wave' includes all vorticity modes.) This is possible when basic shear is relatively strong so that the Doppler-shifted frequency of the Rossby wave has the same value as that of the gravity wave. In this way two waves, which usually have different timescales, can resonate. This new instability is called Rossby–Kelvin (R–K) instability hereinafter. This name indicates the different types of waves that resonate in the lowest mode. This instability seems to have been observed in some studies on frontal instability, but it has not been recognized as an instability caused by resonance between two waves which are usually thought of as having very different frequencies.

This new instability is studied using an ageostrophic version of Phillips' model (two-layer channel model on an f-plane). In §2, basic equations, disturbance energy and disturbance momentum for a two-layer system are described. In §3, a concept for the physical wave coordinate system is discussed. In §4, interaction between wave components is discussed in the framework of physical wave coordinates, and a stability criterion for the two-layer model is deduced. Before discussing the new instability, it is helpful to look at conventional baroclinic and K–H instabilities in terms of the resonance of waves, see §§5 and 6. In §§7 and 8, R–K instability is described in detail. In addition, the ageostrophic baroclinic instability found in the numerical calculations is described in §9.

2. Basic equations, disturbance momentum and energy

We consider a two-layer channel model on an f-plane with vertical shear flow as shown in figure 1. The linearized equations for perturbation are

$$\mathrm{D}_j u_j - f v_j = -\partial_x p_j, \tag{1a}$$

$$\mathrm{D}_j v_j + f u_j = -\partial_y p_j, \tag{1b}$$

$$\mathrm{D}_j h = \pm (H_j \partial_x u_j + \partial_y (H_j v_j)), \tag{1c}$$

$$g' h = p_2 - p_1, \tag{1d}$$

where (x, y) and (u, v) are the (along-channel, cross-channel) coordinates and disturbance velocity components, h is the interface displacement, p is the pressure, D_j is the total derivative $\partial_t + U_j \partial_x$, U_j is the along-channel basic flow, f is the Coriolis parameter, g' is the reduced gravity ($\Delta\rho g$), $H_j = H_0 \mp sy$ is the depth of each layer, H_0 is the average depth, s is the slope of the basic interface, $f(U_1 - U_2)/g'$. Here, $j = 1, 2$ denotes variables for upper and lower layers, the upper sign in $\pm$ corresponds to the upper layer ($j = 1$) and the lower sign to the lower layer ($j = 2$). Boundary conditions for the equations are

$$v_j = 0 \quad \text{at} \quad y = \pm Y_{\max}. \tag{2}$$

This is an ageostrophic version of Phillips' model and both Rossby waves and gravity waves can occur in this system.

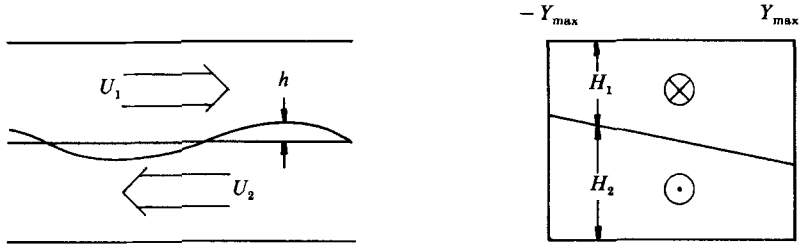

FIGURE 1. Schematic diagrams of the model.

Manipulating (1), we obtain potential vorticity conservation

$$\mathrm{D}_j q_j + v_j \partial_y Q_j = 0, \tag{3}$$

where q_j is the disturbance potential vorticity $(\partial_x v_j - \partial_y u_j \pm Q_j h)/H_j$, and Q_i the basic potential vorticity f/H_j. Therefore potential vorticity is conserved following particles. Introducing the particle displacement, η_j, in the y-direction, equation (3) can be integrated to give

$$q_j = -\eta_j \partial_y Q_j, \tag{4a}$$

$$\mathrm{D}_j \eta_j = v_j, \tag{4b}$$

where it is assumed that q_j is initially zero.

The other important invariants are momentum and energy. In particular, energy analysis has been of central importance to instability theory, and it has been discussed in terms of 'wave' or 'eddy' energy and 'mean' energy. However, we do not have a unique definition of 'wave/eddy' and 'mean' for divergent flow, which makes energy analysis very confusing. For example, Orlanski (1968), Mechoso & Sinton (1983) and Hayashi & Young (1987) defined 'wave/eddy' and 'mean' differently. The author prefers not to use these terms here to avoid confusion and so throughout this paper, discussion is in terms of a 'disturbance' quantity, which is defined by Hayashi & Young (1987). The disturbance quantity is simply defined as the quantity in the disturbed fluid minus that in the undisturbed. (This quantity is called a 'wave' quantity in some literature such as Cairns 1979.) The disturbance energy can be negative simply because a disturbed field does not necessarily have more energy than an undisturbed field, i.e. the field can be disturbed by extracting energy.

Following Hayashi & Young (1987), disturbance momentum M is derived as follows:

$$M = M_{\mathrm{R}} + M_{\mathrm{g}}, \tag{5a}$$

$$M_{\mathrm{R}} = -\tfrac{1}{2}\langle H_1^2(\partial_y Q_1)\,\eta_1^2\rangle - \tfrac{1}{2}\langle H_2^2(\partial_y Q_2)\,\eta_2^2\rangle, \tag{5b}$$

$$M_{\mathrm{g}} = -\langle h u_1\rangle + \langle h u_2\rangle, \tag{5c}$$

where the angle brackets denote a spatial average and (4) is used to derive (5*b*). The basic quantities U_i and Q_i can be arbitrary functions of y. The derivation of (5) is essentially the same as in Hayashi & Young (1987) (see their equation (2.31)) except that the present model has two layers. In Hayashi & Young (1987), M_{R} and M_{g} (M_1 and M_2 in their notation) are called 'mean' momentum and 'wave' momentum. However, the author regards both momenta to be related to waves, because M_{R} and M_{g} are associated with Rossby waves and gravity waves respectively as shown below.

It will also be shown that these momenta have the same sign as those of the intrinsic phase speed $\tilde{c}$ of the waves (the phase speed relative to the basic flow).

From the definition of the disturbance momentum, this does not depend on the frame of reference. In fact, (5) does not include U_1 nor U_2. The disturbance momentum is conserved if there is no external forcing because total momentum remains unchanged without external sources. For an unstable mode, the disturbance momentum must be zero because the disturbance grows without external sources (Hayashi & Young 1987).

Similarly, disturbance energy E is derived as

$$E = E_a + E_b + E_c, \tag{6a}$$

$$E_a = -\tfrac{1}{2}\langle U_1 H_1^2(\partial_y Q_1)\,\eta_1^2\rangle - \tfrac{1}{2}\langle U_2 H_2^2(\partial_y Q_2)\,\eta_2^2\rangle, \tag{6b}$$

$$E_b = -\langle U_1 h u_1\rangle + \langle U_2 h u_2\rangle, \tag{6c}$$

$$E_c = \tfrac{1}{2}\langle H_1(u_1^2+v_1^2)\rangle + \tfrac{1}{2}\langle H_2(u_2^2+v_2^2)\rangle + \tfrac{1}{2}\langle g' h^2\rangle. \tag{6d}$$

The disturbance energy is also conserved if there is no external forcing. Unlike the disturbance momentum, there is no simple classification of these energies E_a, E_b and E_c. In particular, E_a and E_b are not positive definite any more, and these terms have caused the confusion in the energy analysis. For example, in Mechoso & Sinton (1983) the 'wave/eddy' energy includes only E_c, which is positive definite, while in Hayashi & Young (1987) it also includes E_b and it can be negative. Therefore the physical significance of the 'wave/eddy' energy depends entirely on its definition, but there is no physical reason why 'wave/eddy' energy should include E_b.

The disturbance energy E, however, has the following simple relation with the disturbance momentum M (Hayashi & Young 1987):

$$E = cM, \tag{7}$$

where c is the phase speed of the wave observed from a particular frame of reference. This is a great advantage of the 'disturbance' quantity, because we can obtain disturbance energy without the confusing equation (6). Also, this equation fits our physical intuition. Suppose the wave has been excited by a forcing moving at a speed c. The total work done by the forcing is $\int cF\,\mathrm{d}t = cM$, where F is the force applied to the field ($\mathrm{d}M/\mathrm{d}t = F$). Therefore the energy in the disturbed field must differ from that in the undisturbed one by cM.

Once we accept (7), it is obvious that the disturbance energy is not positive definite and it depends on the frame of reference, because c can be chosen arbitrarily by changing the frame of reference while M does not depend on it. This happens even in a simple example, as follows. Suppose a gravity wave packet is propagating in the upstream (positive) direction at an intrinsic phase speed $\tilde{c} > 0$ on a river flowing at a speed of $-U < 0$ in a non-rotating frame. The disturbance momentum ($M \equiv \langle hu\rangle$) of this wave is positive. To excite the wave, we have to move the forcing pattern at speed $c = \tilde{c} - U$, giving positive momentum to the system. When the flow speed of the river is slow enough so that c is positive, the forcing does positive work against the river and therefore the disturbance energy must be positive. When the flow speed of the river exceeds the phase speed, however, the forcing pattern must be moved backward (the opposite direction from the momentum) at negative speed c. This means that the river does work against the forcing and the forcing extracts energy from the system when it excites the wave. Therefore this causes negative disturbance energy. This is physically natural, and negative disturbance energy is not surprising,

although it sounds strange. Again for the unstable mode, the disturbance energy must be zero because an unstable mode grows without external energy input (Hayashi & Young 1987).

Because the disturbance momentum (5) does not depend on the frame of reference and it is separated into two terms by the physical mechanism of the wave, the momentum analysis is more useful for a unique classification of instabilities. Therefore, we shall discuss the interaction of waves mainly in terms of disturbance momentum M or intrinsic phase speed $\tilde{c}$, which has same sign as M, rather than disturbance energy. We can get the disturbance energy from (7) if we need it. Hereafter, the basic flows U_1 and U_2 are set at U_0 and $-U_0$ for simplicity. This causes no loss of generality.

Assuming a sinusoidal form of solution in the x-direction,

$$(u_j(x,y), v_j(x,y), p_j(x,y))^{\mathrm{T}} = \hat{\boldsymbol{z}}_j \exp[\mathrm{i}(kx-\omega t)], \tag{8a}$$

$$\hat{\boldsymbol{z}}_j = (\hat{u}_j(y), \hat{v}_j(y), \hat{p}_j(y))^{\mathrm{T}}, \tag{8b}$$

and substituting (1d) into (1c), (1) is rewritten in a vector form:

$$\hat{D}_1 \hat{\boldsymbol{z}}_1 - \boldsymbol{A}_1 \cdot \hat{\boldsymbol{z}}_1 = \hat{D}_1 \boldsymbol{B} \cdot \hat{\boldsymbol{z}}_2, \tag{9a}$$

$$\hat{D}_2 \hat{\boldsymbol{z}}_2 - \boldsymbol{A}_2 \cdot \hat{\boldsymbol{z}}_2 = \hat{D}_2 \boldsymbol{B} \cdot \hat{\boldsymbol{z}}_1, \tag{9b}$$

where

$$\boldsymbol{A}_j = \begin{pmatrix} 0, & \mathrm{i}f, & k \\ -\mathrm{i}f, & 0, & -\mathrm{i}\partial_y \\ kg'H_j, & -\mathrm{i}g'\,\partial_y(H_j\,\cdot), & 0 \end{pmatrix}, \tag{10a}$$

$$\boldsymbol{B} = \begin{pmatrix} 0, & 0, & 0 \\ 0, & 0, & 0 \\ 0, & 0, & 1 \end{pmatrix}, \tag{10b}$$

where $\hat{D}_j$ is an intrinsic frequency $(\omega \mp kU_0)$, $\partial_y(H_j\,\cdot)$ operates on v_j as $\partial_y(H_j v_j)$, and the superscript T indicates transpose vector or matrix.

3. Physical wave coordinates

Equation (9) is formally a sixth-order eigenvalue problem, although it can be reduced to a fourth-order problem (see Appendix A). If there is no singularity, it is not difficult to solve this problem and get a set of wave modes which are orthogonal to each other in an appropriate norm. However, it is very difficult to understand these modes physically, because each mode includes all physical processes in the system. A great advantage of an orthogonal wave mode system is that each wave mode propagates independently. Namely, taking the set of the eigenvectors $\{\boldsymbol{e}_n\}$ of (9) as the basis of a coordinate system, (9) can be written in the following form:

$$\omega \boldsymbol{x} + \boldsymbol{\Omega} \cdot \boldsymbol{x} = 0, \tag{11}$$

where $\boldsymbol{\Omega}$ is a diagonal matrix, and $\boldsymbol{x} = (X_1, X_2, X_3, \ldots)^{\mathrm{T}}$ is a vector in the coordinate system. Each element of the basis $\boldsymbol{e}_n$ corresponds to a wave mode and X_n represents its amplitude. A solution of this problem is expressed by summation of these free modes. Equation (11) is mathematically simple and beautiful, but it tells us nothing about the physical mechanism of the wave mode. If we do not mind accounting for interaction between wave modes, however, we can project (11) onto any coordinate

system with respect to an arbitrary basis. In general (9) can be written in an arbitrary coordinate system with respect to a basis $\{\boldsymbol{e}'_n\}$ as follows:

$$\omega \boldsymbol{x}' + \boldsymbol{\Omega}' \cdot \boldsymbol{x}' = \omega \boldsymbol{B}_1 \cdot \boldsymbol{x}' + \boldsymbol{B}_2 \cdot \boldsymbol{x}', \tag{12}$$

where $\boldsymbol{x}'$ is a vector in the coordinate system, $\boldsymbol{\Omega}'$ is a diagonal matrix and $\boldsymbol{B}_1$ and $\boldsymbol{B}_2$ are matrices in which all diagonal components are 0. In this coordinate system, the wave mode $\boldsymbol{e}_n$ is expressed by a summation $\Sigma X'_i \boldsymbol{e}'_i$. Although (12) is more complicated than (11), it can be useful in understanding the physics of the wave mode if each component of the coordinate has a physical meaning. For example, if $\boldsymbol{e}'_i$ represents a free wave in a subsystem of (9), which is simpler than (9), the wave mode in the full system (9) can be interpreted in terms of the interaction between the simple waves.

If we assume $p_2 = 0$ in (1) or $\boldsymbol{B} = 0$ in (9), the equations for the upper layer reduce to those of a one-layer system where we understand the physics of the eigenfunctions much better than in a two-layer system. The equation for this system is

$$\hat{D}_1 \hat{\boldsymbol{z}}_1 - \boldsymbol{A}_1 \cdot \hat{\boldsymbol{z}}_1 = 0, \tag{13}$$

where $\hat{D}_1$ is an intrinsic frequency $(\omega - kU_0)$ and $\boldsymbol{A}_1$ is defined in (10). If we look at this system moving with the basic velocity flow U_0, (13) is equivalent to the equation for waves in a channel with sloping bottom and no basic flow. Each eigenvector of (13) $\boldsymbol{e}_{1n}$ corresponds to a topographic Rossby wave or a gravity wave, and any disturbance can be written as a summation of these waves, i.e. we can define a coordinate system with respect to $\boldsymbol{e}_{1n}$. It is the same for the lower layer and we can define a coordinate system with respect to the eigenvectors of the lower layer $\{\boldsymbol{e}_{2n}\}$. Since we are familiar with the characteristics of these waves, at least we know what the dispersion curves for the waves look like, it is physically natural to use a coordinate system with respect to $\{\boldsymbol{e}_{1n}\} \cup \{\boldsymbol{e}_{2n}\}$ which consists of two sets of coordinates for two one-layer systems. To avoid confusion of the two coordinate systems: $\{\boldsymbol{e}_n\}$ and $\{\boldsymbol{e}_{1n}\} \cup \{\boldsymbol{e}_{2n}\}$, the former is called the mathematical coordinate or wave mode and the latter is called the physical coordinate or wave component.

The physical wave coordinate system in the present model is defined as follows. The adjoint equation of (13) is given by

$$\hat{D}_1^* \hat{\boldsymbol{z}}_1 - \bar{\boldsymbol{A}}_1 \cdot \hat{\boldsymbol{z}}_1 = 0, \tag{14a}$$

$$\bar{\boldsymbol{A}}_1 \equiv \begin{pmatrix} 0, & \mathrm{i}f, & kg'H_1 \\ -\mathrm{i}f, & 0, & -\mathrm{i}g'H_1 \partial_y \\ k, & -\mathrm{i}\partial_y, & 0 \end{pmatrix}, \tag{14b}$$

where * denotes complex conjugate and $\bar{\boldsymbol{A}}_1$ is the adjoint operator. Suppose $\boldsymbol{e}_{1n} = (u_{1n}, v_{1n}, p_{1n})^{\mathrm{T}}$ is an eigenvector of (13). The eigenvector of (14) is given by

$$\begin{aligned} \bar{\boldsymbol{e}}_{1n} &\equiv (\bar{u}_{1n}, \bar{v}_{1n}, \bar{p}_{1n})^{\mathrm{T}} \\ &= \left(H_1 u_{1n}, H_1 v_{1n}, \frac{1}{g'} p_{1n}\right)^{\mathrm{T}}, \end{aligned} \tag{15}$$

and satisfies

$$\int \bar{\boldsymbol{e}}_{1n}^{*\mathrm{T}} \cdot \boldsymbol{e}_{1m} = d_{1n}^2 \delta_{nm}, \tag{16a}$$

$$d_{1n}^2 \equiv \int (\bar{u}_{1n}^* u_{1n} + \bar{v}_{1n}^* v_{1n} + \bar{p}_{1n}^* p_{1n})\,\mathrm{d}y$$

$$= \int \left(H_1 u_{1n}^* u_{1n} + H_1 v_{1n}^* v_{1n} + \frac{1}{g'} p_{1n}^* p_{1n} \right) \mathrm{d}y, \tag{16b}$$

where δ_{nm} is Kronecker's delta. Therefore, the amplitude X_n, which is a component of the wave coordinate, is written as

$$X_n = \frac{1}{d_{1n}} \int \bar{\boldsymbol{e}}_{1n}^{*\mathrm{T}} \cdot \hat{\boldsymbol{z}}_1 \,\mathrm{d}y$$

$$= \frac{1}{d_{1n}} \int (\bar{u}_{1n}^* \hat{u}_1 + \bar{v}_{1n}^* \hat{v}_1 + \bar{p}_{1n}^* \hat{p}_1)\,\mathrm{d}y. \tag{17}$$

The original variables are recovered by

$$\hat{\boldsymbol{z}}_1 \equiv (\hat{u}_1(y), \hat{v}_1(y), \hat{p}_1(y))^{\mathrm{T}}$$

$$= \Sigma \frac{1}{d_{1n}} X_n \boldsymbol{e}_{1n}$$

$$= \Sigma \frac{1}{d_{1n}} X_n (u_{1n}, v_{1n}, p_{1n})^{\mathrm{T}}. \tag{18}$$

The wave component in the lower layer ($\boldsymbol{e}_{2n}$) and its corresponding coordinate are obtained in the same manner. To eliminate the suffix for the layer number, the wave coordinate for lower layer is denoted as $\boldsymbol{y} = (Y_1, Y_2, Y_3, \ldots)^{\mathrm{T}}$.

If we discretize in the y-direction using N points, we have $6N$ wave coordinates ($3N$ for each layer) and $6N$ eigenvalues. However, these eigenvalues include $2N$ of infinite value, and the present model reduces to an eigenvalue problem in $4N$-dimensional space (see Appendix B). This is because the interaction between waves introduces some restriction on the freedom of the solutions. Physically speaking, the internal surface is not independent for the upper and lower layers and we have excluded external gravity modes from (9) by considering a rigid upper boundary. Therefore we shall discuss a $4N$-dimensional subspace, which is spanned by orthogonal wave modes, in a $6N$-dimensional coordinate system.

4. Interaction between wave components

In the physical coordinate system defined above, each wave component does not interact with the other components in the same layer, but does interact with those in the other layer through pressure (see (9*b*)). As shown in Appendix A, (9) can be rewritten in the physical coordinates as

$$\hat{D}_1 X_n - \tilde{\omega}_{1n} X_n = \hat{D}_1 \sum_m \epsilon_{nm} Y_m, \tag{19a}$$

$$\hat{D}_2 Y_m - \tilde{\omega}_{2m} Y_m = \hat{D}_2 \sum_n \epsilon_{nm}^* X_n, \tag{19b}$$

$$\epsilon_{nm} = \frac{1}{g' d_{1n} d_{2n}} \int p_{1n}^* p_{2m} \,\mathrm{d}y, \tag{19c}$$

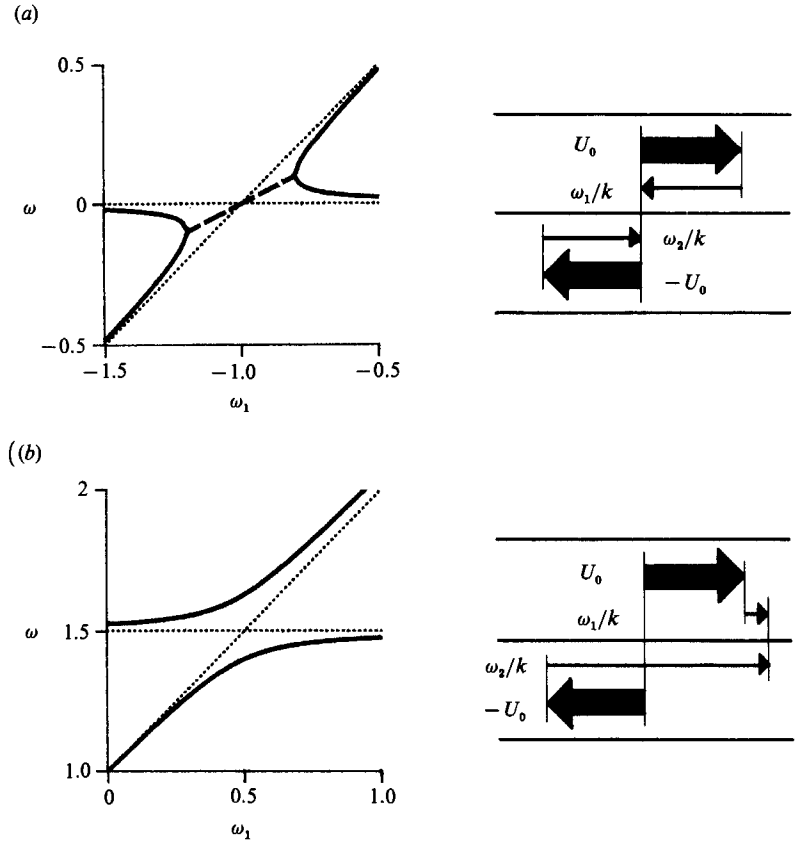

FIGURE 2. Frequency of the wave modes when two wave components have almost the same frequencies (solid lines in left-hand panels) for (*a*) $\tilde{\omega}_1\tilde{\omega}_2 < 0$ and (*b*) $\tilde{\omega}_1\tilde{\omega}_2 > 0$. Dotted lines shows Doppler-shifted frequencies $\tilde{\omega}_1 + kU_0$ and $\tilde{\omega}_2 - kU_0$ and the broken line shows the unstable mode. Right panels show schematically the relation between U_0, $\tilde{\omega}_1$ and $\tilde{\omega}_2$. $kU_0 = 1$, $\omega_2 = 1$ for (*a*), $\tilde{\omega}_2 = 2.5$ for (*b*) and only $\tilde{\omega}_1$ is varied.

where $\tilde{\omega}_{1n}$ and $\tilde{\omega}_{2m}$ are the intrinsic frequencies of free modes in a one-layer system for the upper and lower layer, X_n and Y_m are the amplitudes of the modes in the upper and lower layer. The absolute value of the interaction coefficient ϵ_{nm} is less than 1 (Appendix A). The basic interaction between two components can be written as

$$\hat{D}_1 X - \tilde{\omega}_1 X = \epsilon \hat{D}_1 Y, \tag{20a}$$

$$\hat{D}_2 Y - \tilde{\omega}_2 Y = \epsilon^* \hat{D}_2 X. \tag{20b}$$

These equations reduce to

$$\left(\omega - \frac{\tilde{\omega}_1 + \tilde{\omega}_2}{2(1-\epsilon\epsilon^*)}\right)^2 - \mu = 0, \tag{21a}$$

where

$$\mu = \left(kU_0 + \frac{\tilde{\omega}_1 - \tilde{\omega}_2}{2(1-\epsilon\epsilon^*)}\right)^2 + \frac{\epsilon\epsilon^*}{(1-\epsilon\epsilon^*)^2}\tilde{\omega}_1\tilde{\omega}_2. \tag{21b}$$

Now we assume that $\tilde{\omega}_1$ and $\tilde{\omega}_2$ are real (these components are stable). In the present case, this is assured by Ripa's theorem for a one-layer system. The theorem

guarantees stability if there is an α such that $Q_y(\alpha-U) \geqslant 0$ and $H \geqslant (\alpha-U)^2$ for all y. A constant $\alpha = U$ satisfies these conditions and therefore this system is stable.

When $\tilde{\omega}_1\tilde{\omega}_2 > 0$, μ is always positive and (21) gives real ω. Therefore, the wave modes are stable. When $\tilde{\omega}_1\tilde{\omega}_2 < 0$, μ is negative for $kU_0 = -(\tilde{\omega}_1-\tilde{\omega}_2)/(1-\epsilon^2)$ and (21) gives complex eigenvalues. If ϵ is small enough, the instability occurs when $\tilde{\omega}_1+kU_0 \approx \tilde{\omega}_2-kU_0$. These situations are schematically shown in figure 2. The condition for stability can be summarized as follows.

The flow is unstable if there is a pair of wave components such that:

(i) they propagate in the opposite direction to the basic flow ($\tilde{\omega}_1\tilde{\omega}_2 < 0$);

(ii) they have almost the same Doppler-shifted frequency ($\tilde{\omega}_1+kU_0 \approx \tilde{\omega}_2-kU_0$);

(iii) they can interact with each other ($\epsilon_{nm} \neq 0$).

This is identical with the stability criterion of Hayashi & Young (1987). Note that conditions (i) and (iii) hold even when ϵ_{nm} is not small. As shown later, both gravity waves and Rossby waves have disturbance momentum in the direction of the phase speed relative to the basic flow. Therefore condition (i) can be rewritten as that two waves have disturbance momentum in opposite directions. With the combination of such wave components, the disturbance momentum of the sum can be zero and can grow without external forcing. The amplitudes of wave components in the unstable mode are determined so that the disturbance momentum for the wave mode is zero. The disturbance energy for the unstable mode is automatically zero because of (7).

5. Baroclinic instability and Rossby waves

In this and the next section, conventional baroclinic instability and Kelvin–Helmholtz instability are described in the physical wave coordinate system as examples of the instabilities caused by the resonance of waves.

In this section, (9) is considered in a geostrophic limit, and the baroclinic instability is interpreted as a resonance between Rossby waves. Before considering the interaction, we have to obtain the wave components in each layer by solving the equation for a one-layer system (13) instead of (9). If the variation of the depth of the layers $\Delta H = sY_{\max}$ is small (the channel is narrow), the matrix $\boldsymbol{A}_1$ becomes independent of y and we can assume the solution in the upper layer has following form:

$$\hat{z}_1 = X_n(u', v', p')^{\mathrm{T}} \exp(\mathrm{i}l_n y), \tag{22}$$

where u', v' and p' are independent of y. Substituting (22) into (13) with the quasi-geostrophic approximation, we get an equation for a Rossby wave,

$$\hat{D}_1 X_n - \tilde{\omega}_{1n} X_n = 0, \tag{23a}$$

where

$$\tilde{\omega}_{1n} = \frac{-2kU_0}{2R^2|\boldsymbol{k}|^2+1}, \tag{23b}$$

$$R = \frac{(\frac{1}{2}g'H_0)^{\frac{1}{2}}}{f}, \tag{23c}$$

$$\boldsymbol{k} = (k, l_n), \tag{23d}$$

and the corresponding eigenvector is

$$\boldsymbol{e}_{1n} = \left(\frac{\mathrm{i}l_n}{f}, -\frac{\mathrm{i}k}{f}, 1\right)^{\mathrm{T}} \exp(\mathrm{i}l_n y). \tag{24}$$

This set of Rossby waves forms the physical wave coordinate system. In this coordinate system, the disturbance is expressed in a vector form,

$$\boldsymbol{x} = (X_1, X_2, \ldots)^{\mathrm{T}}. \tag{25}$$

Namely, the disturbance is a superposition of Rossby waves. These Rossby waves in the upper layer have negative intrinsic phase speed.

The Rossby wave components in the lower layer are obtained in the same manner. The eigenvector for the lower layer has the same form as that in the upper layer and its intrinsic frequency is of opposite sign,

$$\boldsymbol{e}_{2n} = \left(\frac{\mathrm{i}l_n}{f}, -\frac{\mathrm{i}k}{f}, 1\right)^{\mathrm{T}} \exp(\mathrm{i}l_n y), \tag{26a}$$

$$\tilde{\omega}_{2n} = -\tilde{\omega}_{1n} = \frac{2kU_0}{2R^2|\boldsymbol{k}|^2+1}. \tag{26b}$$

The dispersion curves for the waves in both layers are shown by broken lines in figure 3. These dispersion curves intersect at $k = 1/(\sqrt{2}R)$ and $k = 0$. From the discussion of previous sections, we can expect instability around the intersection points.

Substituting (23) and (26) into (19c), the interactions between Rossby waves are expressed from (19) as follows:

$$\hat{D}_1 X_n - \tilde{\omega}_{1n} X_n = \epsilon_n \hat{D}_1 Y_n, \tag{27a}$$

$$\hat{D}_2 Y_n + \tilde{\omega}_{1n} Y_n = \epsilon_n D_2 X_n, \tag{27b}$$

$$\epsilon_n = \frac{1}{2R^2|\boldsymbol{k}|^2+1}. \tag{27c}$$

A wave component in the upper layer can interact only with a lower component that has the same spatial structure, because others are orthogonal. Eliminating X_n and Y_n in (27), we obtain the frequency of the wave mode as

$$\omega = \pm kU_0\left(1 - \frac{2}{R^2|\boldsymbol{k}|^2+1}\right)^{\frac{1}{2}}. \tag{28}$$

Note that we have not solved the full equation (9) directly to get (28). We have only solved the equations for subsystem (13), which is much easier. The wave coordinate system in this section is identical with the Fourier transform, which is used in Phillips (1954) and Pedlosky (1979), because each wave component has sinusoidal form. The wave coordinate system, however, can be applied even when the wave does not have sinusoidal form and the Fourier transformation fails to simplify the problem.

The dispersion curves of wave modes are shown by heavy solid lines in figure 3. When $|\boldsymbol{k}|$ is sufficiently small, the wave mode becomes unstable because of the interaction. As $|\boldsymbol{k}|$ becomes large, dispersion curves of wave modes asymptotically approach those of the wave components. This is because the interaction coefficient ϵ_n becomes smaller and the difference of the Doppler-shifted frequencies in both layers becomes large.

Using (26), the ratio of wave components in a wave mode is given by

$$\frac{X_n}{Y_n} = \left(\frac{(kU_0-\omega)(\tilde{\omega}_n+kU_0+\omega)}{(kU_0+\omega)(\tilde{\omega}_n+kU_0-\omega)}\right)^{\frac{1}{2}}. \tag{29}$$

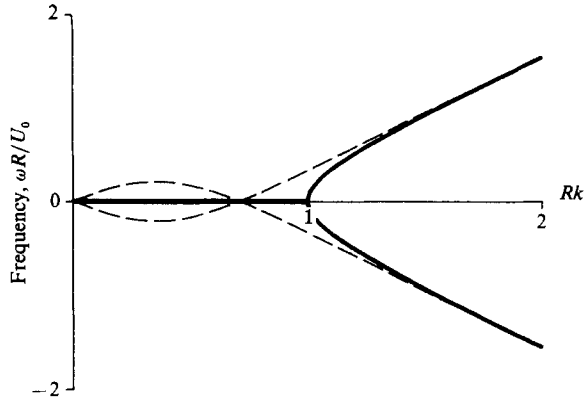

FIGURE 3. Frequencies of the Rossby wave components (broken lines) and wave modes (heavy solid line) when $l = 0$.

When $\boldsymbol{k}$ is sufficiently large ($\omega \approx \pm kU_0$), the wave mode is almost identical with the wave component ($X_n/Y_n \to 0$ or ∞). When $\boldsymbol{k}$ is small and the wave mode is unstable, ω is pure imaginary and two wave components have same amplitude ($|X_n/Y_n| = 1$).

From (5), the mean momentum and wave momentum for the wave component in the upper layer are

$$M_{\mathrm{R}} = -\langle \tfrac{1}{2} H_1^2 \eta_1^2 \partial_y Q_1 \rangle = -\frac{f^2 U_0}{g'} \langle \eta_1^2 \rangle, \tag{30a}$$

$$M_{\mathrm{g}} = 0. \tag{30b}$$

Therefore the Rossby wave in the upper layer has disturbance momentum ($M = M_{\mathrm{R}} + M_{\mathrm{g}}$) in the direction of the intrinsic phase speed (negative direction). Similarly the Rossby wave in the lower layer has positive intrinsic phase speed and positive disturbance momentum. For the unstable modes, disturbance momentum vanishes because the two wave components have disturbance momentum in opposite directions and have the same amplitude.

6. Gravity waves and Kelvin–Helmholtz instability

We consider a two-layer channel system in a non-rotating frame ($f = 0$ and $H_1 = H_2 = H_0$). Again we solve the equations for a one-layer system (13) to obtain wave components in the upper layer. Suppose the solution has a plane-wave form and is propagating only in the x-direction, viz.

$$\hat{\boldsymbol{z}}_1 = (u', 0, p')^{\mathrm{T}}, \tag{31}$$

where u', p' are independent of y. From (13) we obtain the intrinsic frequency of the wave components,

$$\tilde{\omega}_1^+ = k(g'H_0)^{\frac{1}{2}}, \tag{32a}$$

$$\tilde{\omega}_1^- = -k(g'H_0)^{\frac{1}{2}}. \tag{32b}$$

The corresponding eigenvectors are

$$\boldsymbol{e}_1^+ = (1, 0, (g'H_0)^{\frac{1}{2}})^{\mathrm{T}}, \tag{33a}$$

$$\boldsymbol{e}_1^- = (1, 0, -(g'H_0)^{\frac{1}{2}})^{\mathrm{T}}. \tag{33b}$$

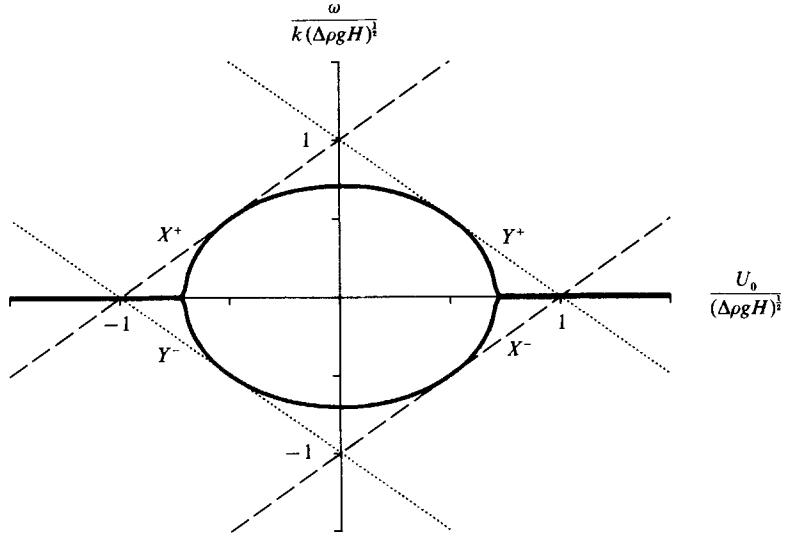

FIGURE 4. Frequencies of the gravity wave components and wave modes. The wave components in the upper layer are indicated by broken lines and the wave components in the lower layer are indicated by dotted lines. The heavy solid line indicates the frequency of the wave mode.

The wave components for the lower layer are obtained similarly. Because $\boldsymbol{A}_2 = \boldsymbol{A}_1$, the eigenvectors and their intrinsic frequencies in the lower layer are exactly the same as those in the upper layer:

$$\tilde{\omega}_2^+ = \tilde{\omega}_1^+ = k(g'H_0)^{\frac{1}{2}}, \tag{34a}$$

$$\tilde{\omega}_2^- = \tilde{\omega}_1^- = -k(g'H_0)^{\frac{1}{2}}, \tag{34b}$$

$$\boldsymbol{e}_2^+ = \boldsymbol{e}_1^+ = (1, 0, (g'H_0)^{\frac{1}{2}})^{\mathrm{T}}, \tag{34c}$$

$$\boldsymbol{e}_2^- = \boldsymbol{e}_1^- = (1, 0, -(g'H_0)^{\frac{1}{2}})^{\mathrm{T}}. \tag{34d}$$

The phase speeds of wave components for the upper and lower layers are shown in figure 4. X^+ and X^- are wave components in the upper layer and Y^+ and Y^- are wave components in the lower layer. Superscripts + and − indicate the direction of the intrinsic phase speed. These phase speeds intersect at $|U_0| = 0$ and $(g'H_0)^{\frac{1}{2}}$. From the previous section, we can expect an instability at $|U_0| = (g'H_0)^{\frac{1}{2}}$, because wave components in resonance have phase speeds in the opposite direction to the basic flow.

Substituting (33) and (34) into (19c), we get

$$\hat{D}_1 X^+ - \tilde{\omega}^+ X^+ = \hat{D}_1(\epsilon Y^+ - \epsilon Y^-), \tag{35a}$$

$$\hat{D}_1 X^- - \tilde{\omega}^- X^- = \hat{D}_1(-\epsilon Y^+ + \epsilon Y^-), \tag{35b}$$

$$\hat{D}_2 Y^+ - \tilde{\omega}^+ Y^+ = \hat{D}_2(\epsilon X^+ - \epsilon X^-), \tag{35c}$$

$$\hat{D}_2 Y^- - \tilde{\omega}^- Y^- = \hat{D}_2(-\epsilon X^+ + \epsilon X^-), \tag{35d}$$

$$\epsilon = \tfrac{1}{2}. \tag{35e}$$

The frequency of the wave mode in the two-layer system (35) is given by

$$\omega = \pm k(\tfrac{1}{2}g'H_0 - U_0^2)^{\frac{1}{2}}. \tag{36}$$

The phase speeds of these wave modes are shown by heavy lines in figure 4. As expected, the wave modes become unstable near the intersection points $|U_0| = (g'H_0)^{\frac{1}{2}}$. Although there are four wave components, there are only two wave modes, because we have excluded external modes by the rigid-lid boundary condition at the top surface. The barotropic pressure field (p_1+p_2) can propagate at infinite speed and therefore its curve has disappeared from figure 4.

When $U_0 = \frac{1}{2}(g'H_0)^{\frac{1}{2}}$, the frequency of the wave mode is tangent to that of the wave components. At this point (35) reduces to

$$\hat{D}_1 X^- - \tilde{\omega}^- X^- = 0, \tag{37a}$$

$$\hat{D}_2 Y^+ - \tilde{\omega}^- Y^+ = 0, \tag{37b}$$

$$X^+ = Y^- = 0. \tag{37c}$$

This means that the wave components X^- and Y^+ can be propagated without interaction. Therefore each wave mode consists of only one component. This is because the disturbance of the interface due to the wave component X^- in the upper layer is seen from lower layer to be at rest. The fluid in the lower layer is just advected by the basic flow. This point is very important when we consider the full equations of motion (1), because the Rossby wave, which has very small intrinsic phase speed, can interact with the gravity wave in the other layer.

The momenta for these wave components are

$$M_{\mathrm{R}} = 0, \tag{38a}$$

$$M_{\mathrm{g}} = \pm\left(\frac{H}{g'}\right)^{\frac{1}{2}} \langle u_j^2 \rangle. \tag{38b}$$

Again the wave components have disturbance momenta in the direction of their intrinsic phase velocity.

7. Rossby–Kelvin instability

Scaling time by $1/f$, x and y by $R = (g'H_0/2)^{\frac{1}{2}}/f$, h by H_0, non-dimensional equations are

$$\hat{D}_1' z_1' - \boldsymbol{A}_1' \cdot z_1' = \hat{D}_1' \boldsymbol{B}' \cdot z_2', \tag{39a}$$

$$\hat{D}_2' z_2' - \boldsymbol{A}_2' \cdot z_2' = \hat{D}_2' \boldsymbol{B}' \cdot z_1', \tag{39b}$$

$$\boldsymbol{A}_j' = \begin{pmatrix} 0, & \mathrm{i}, & k' \\ -\mathrm{i}, & 0, & -\mathrm{i}\partial_y' \\ 2k'H', & -2\mathrm{i}H'\partial_y' \pm 2\mathrm{i}F, & 0 \end{pmatrix}, \tag{39c}$$

$$\boldsymbol{B}' = \begin{pmatrix} 0, & 0, & 0 \\ 0, & 0, & 0 \\ 0, & 0, & 1 \end{pmatrix}, \tag{39d}$$

where $\hat{D}_j' = \mathrm{i}(\omega \mp kF)$, F is Froude number $(F \equiv U_0/(\frac{1}{2}g'H_0)^{\frac{1}{2}})$ H_j' is the non-dimensional depth $H_j' = 1 \mp Fy$, and a prime indicates non-dimensional variables. For clarity, hereafter the prime is dropped and only non-dimensional variables are used.

In non-dimensional units, the Kelvin wave component has an intrinsic phase speed of $\approx \pm\sqrt{2}$, and F can be thought of as the basic velocity. When $F \sim 1/\sqrt{2}$ $(U_0 \sim \frac{1}{2}(g'H_0)^{\frac{1}{2}})$, the Kelvin wave in the upper layer has a negative phase speed of

$\sim -1/\sqrt{2}$, which is the basic velocity in the lower layer. In the lower layer we have a group of Rossby waves which have a small positive intrinsic phase speed. Therefore, an instability is possible because of the resonance between the Kelvin wave in the upper layer and the Rossby waves in the lower layer.

If we neglect wave components that have different frequencies far from the resonance, (19) becomes

$$\hat{D}_1 X - \tilde{\omega}_0 X = \hat{D}_1(\epsilon_1 Y_1 + \epsilon_2 Y_2 + \ldots + \epsilon_n Y_n), \tag{40a}$$

$$\hat{D}_2 Y_1 - \tilde{\omega}_1 Y_1 = \hat{D}_2 \epsilon_1^* X, \tag{40b}$$

$$\hat{D}_2 Y_2 - \tilde{\omega}_2 Y_2 = \hat{D}_2 \epsilon_2^* X, \tag{40c}$$

$$\vdots$$

$$\hat{D}_2 Y_n - \tilde{\omega}_n Y_n = \hat{D}_2 \epsilon_n^* X, \tag{40d}$$

where X is the amplitude of Kelvin wave in the upper layer and Y_n is the amplitude of nth Rossby wave. Neglecting the variation of the depth H_j and assuming the following form of the wave components and frequencies:

$$\boldsymbol{e}_0 \sim (-1, 0, \sqrt{2})^{\mathrm{T}} \exp\left(\frac{y}{\sqrt{2}}\right), \tag{41a}$$

$$\boldsymbol{e}_n \sim (-l_n \cos l_n(y + Y_{\max}), k \sin l_n(y + Y_{\max}), \sin l_n(y + Y_{\max}))^{\mathrm{T}}, \tag{41b}$$

$$\tilde{\omega}_0 \sim -k\sqrt{2}, \tag{41c}$$

$$\tilde{\omega}_n \sim \frac{2kF}{2(k^2 + l_n^2) + 1}, \tag{41d}$$

we can roughly estimate the interaction coefficient ϵ_n:

$$\epsilon_n \approx \frac{2l_n}{(2l_n^2 + 1)[Y_{\max}(2(k^2 + l_n^2) + 1)]^{\frac{1}{2}}}, \tag{42}$$

where the relatively small quantity $\exp(-Y_{\max})$ is neglected. Equation (42) indicates that the lower-mode Rossby waves interact with the Kelvin wave more strongly than do the higher modes.

Figure 5 shows the solution of (40) for three Rossby components ($n = 1, 2, 3$) with $Y_{\max} = 1/\sqrt{2}, k = 2.5$. In this figure, $\tilde{\omega}_0$, $\tilde{\omega}_n$ and ϵ_n are fixed while only F and $\hat{D}_1$ and $\hat{D}_2$ is varied from 0.6 to 0.9. The dotted line shows the phase speed of each wave component. The phase speed of the Kelvin wave component increases as F increases, and the phase speeds of Rossby wave components decrease. Except around a point where these curves intersect, each wave mode is almost identical with a wave component. Between points P and Q in the figure, however, it is somewhat complicated. As F increases, the Kelvin wave component starts to interact with the third Rossby component creating one unstable mode, and it bifurcates into a Kelvin wave mode and a first Rossby mode at a point Q. The stable Rossby wave modes are smoothly substituted for the next modes between P and Q. Each wave mode is a mixture of all wave components in resonance there.

The phase speed of the Kelvin wave mode is shifted downward by the interaction. This is because the existence of the Rossby wave 'stiffens' the lower layer and the restoring force is slightly increased. Therefore, the absolute value of the phase speed of the Kelvin mode is increased by the interaction.

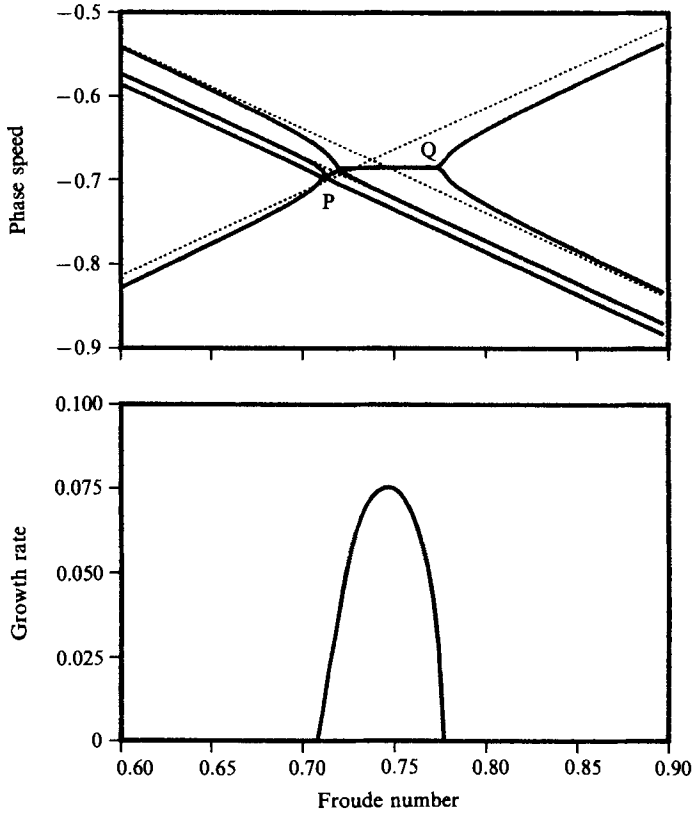

FIGURE 5. Resonance between Rossby waves and a Kelvin wave, calculated from (40) and (42) for $Y_{\max} = 1/\sqrt{2}, k = 2.5$. Dotted line shows the phase speed of each wave component.

8. Numerical confirmation

Equation (39) is directly solved by discretizing the y-interval following Hayashi & Young (1987). For details of the numerical calculation, see Appendix B. Although we have three parameters (k, $Y_{\max}$ and F), $\Delta H \equiv F Y_{\max}$ is fixed at a constant value so that we can survey over a wide range of (k, F)-space. When $\Delta H \geqslant 1$, the interface intersects with the surface and the bottom.

Figure 6 shows the maximum growth rate for $\Delta H = 0.5$. Clearly, several types of instability can be seen. At the lower-left corner, baroclinic instability occurs. At the top, Kelvin–Helmholtz (K–H) instability occurs. The R–K instability occurs at $F \sim (1/2)^{\frac{1}{2}}$ due to the resonance between Rossby waves and a Kelvin wave. The branch at the upper right is an instability caused by a resonance between Rossby waves and the first Poincaré wave.

Dispersion curves for the waves along the section indicated by the dashed line in figure 6 are shown in figure 7. The waves change their scale, keeping the aspect ratio $k/l_0 \sim 1$ ($l_0 = \pi/Y_{\max}$) along this section. In this figure the Rossby waves have a phase speed $\approx \pm F$, which is the velocity of the basic flow, and resonate at low wavenumber to produce a baroclinic instability. The phase speed of the Kelvin wave is about ± 1 at low Froude number and decreases as the Froude number increases. The Kelvin waves resonate at high Froude number ($F \approx 1$) to produce K–H instability. The

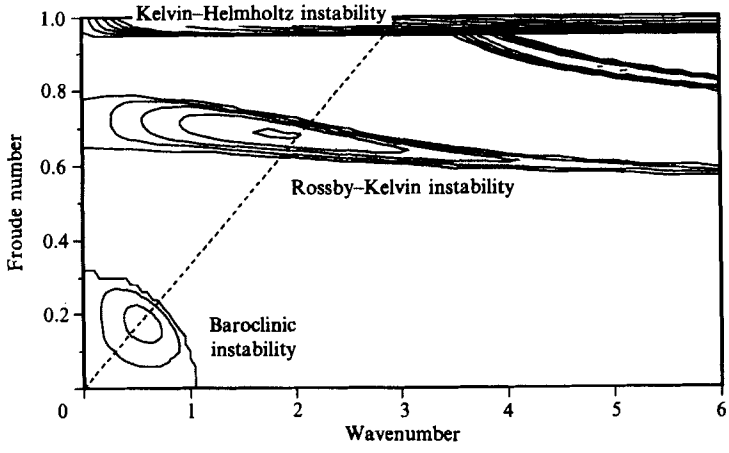

FIGURE 6. Maximum growth rate for $\Delta H \equiv FY_{\max} = 0.5$. The dashed line indicates the section shown in figure 5. Contour interval is 0.02.

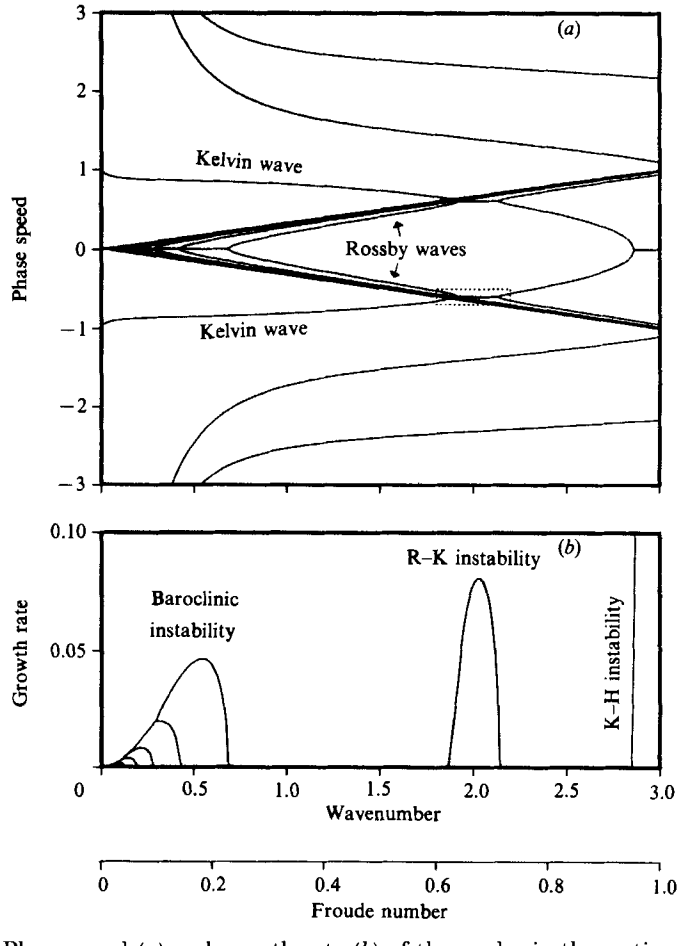

FIGURE 7. Phase speed (a) and growth rate (b) of the modes in the section ($3F = k$) indicated by a dashed line in figure 6. The small area boxed by a dotted line is shown in figure 8.

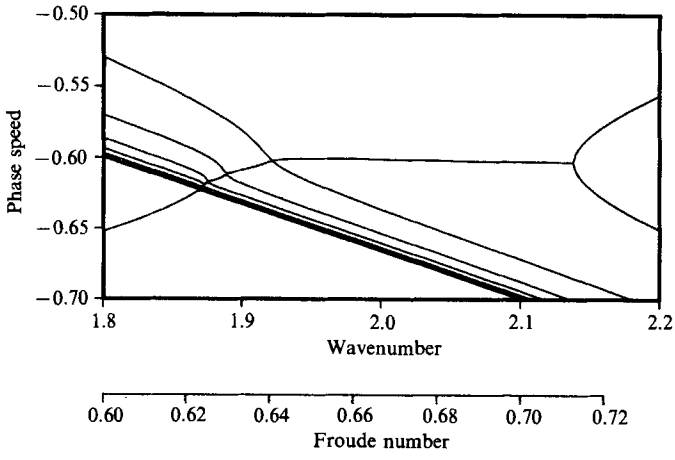

FIGURE 8. Detail of the resonance between a Kelvin wave and Rossby waves.

resonance between Rossby waves and the Kelvin wave is also clearly seen at the intermediate value of the Froude number ($F \approx 0.7$). At this point, the Kelvin wave component interacts with all Rossby wave components resulting in only one unstable mode. Figure 8 shows the resonance in detail. This figure agrees well with figure 5.

The pressure fields and the interface height for the unstable mode at maximum growth rate are shown in figure 9. The reader can clearly recognize a Kelvin wave in the upper layer. In the lower layer the velocity is almost parallel to the pressure contour lines. This pattern of the wave is almost a superposition of just the first and second Rossby wave components. To measure the geostrophy, a geostrophic index G_j is defined as follows:

$$G_j = \left\langle \frac{fv_j(\partial_x p_j) - fu_j(\partial_y p_j)}{(\partial_x p_j)^2 + (\partial_y p_j)^2} \right\rangle. \tag{43}$$

When the flow is in complete geostrophic balance, $G = 1$. The geostrophic indexes are 1.005 for the lower layer and 0.211 for the upper layer. The flow in the lower layer is in almost complete geostrophic balance.

The wave amplitude in the lower layer is much smaller than that in the upper layer and therefore the pattern of the interface height is similar to the pressure in the upper layer. (Note that the contour-line intervals differ by an order of magnitude between the upper and lower layers.) This is because the Rossby wave is much more effective in containing the disturbance momentum than is the Kelvin wave. The disturbance momentum for the Rossby wave in the lower layer is estimated in non-dimensional units as

$$\begin{aligned} m \approx M_{\mathrm{R}} &= \tfrac{1}{2}F\langle \eta_2^2 \rangle \\ &\approx \tfrac{1}{2}F\frac{\langle v_2^2 \rangle}{\tilde{\omega}_2^2} \\ &= \tfrac{1}{2}F\frac{(k^2+l^2+1)^2}{k^2F^2}\langle v_2^2 \rangle. \end{aligned} \tag{44}$$

Provided that $3F = k \approx l$, the disturbance momentum for the first Rossby wave component on this section is given by

$$m \approx 18F\langle v_2^2 \rangle. \tag{45}$$

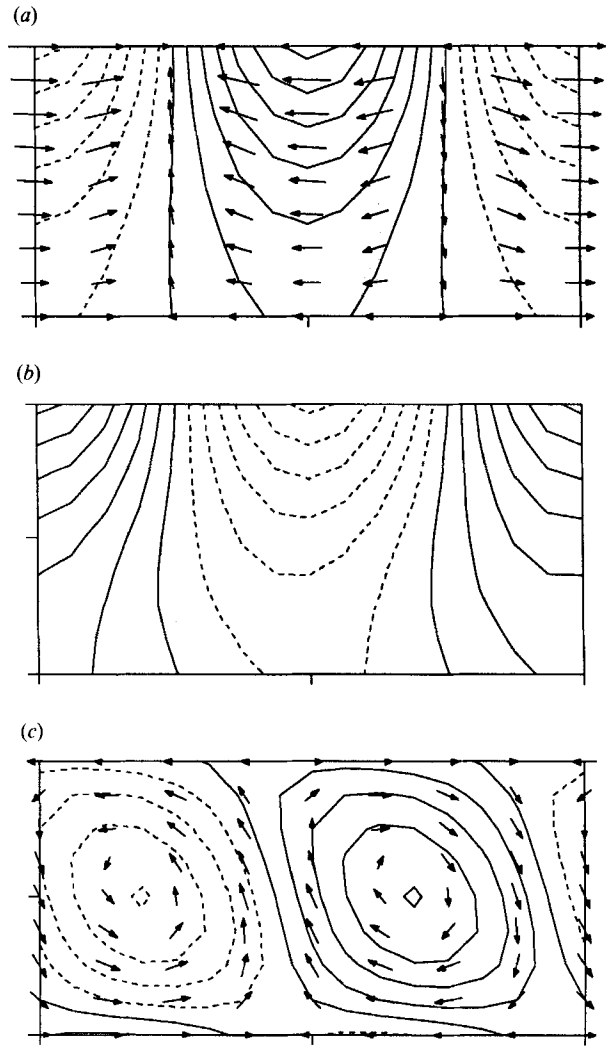

FIGURE 9. Pressure and velocity fields of R–K instability in (*a*) the upper layer and (*c*) the lower layer at the maximum growth rate ($F = 0.675$, $k = 2.025$). Interface height is shown in (*b*). The dotted lines indicate negative contours. The geostrophic indexes are (*a*) 0.211 and (*c*) 1.005. The contour intervals are (*a*) 0.2, (*b*) 0.1 and (*c*) 0.02. The length of the arrows is proportional to $|(u_j, v_j)|^{0.4}$.

The non-dimensional disturbance momentum for a Kelvin wave in the upper layer is

$$m \approx M_g = \langle hu_1 \rangle \approx -\langle \sqrt{2u_1^2} \rangle. \tag{46}$$

The disturbance momentum for a Rossby wave is larger by one order of magnitude than that of a Kelvin wave with the same amplitude when Rossby–Kelvin instability occurs ($F \approx 0.7$). Therefore the Kelvin wave component must dominate the Rossby wave component in the unstable mode to cancel the disturbance momentum. The disturbance momenta for modes with negative phase speeds are shown in figure 10. (Note that the scale for negative momentum is exaggerated by 10). The disturbance momenta of Rossby modes are positive and almost proportional to F. The

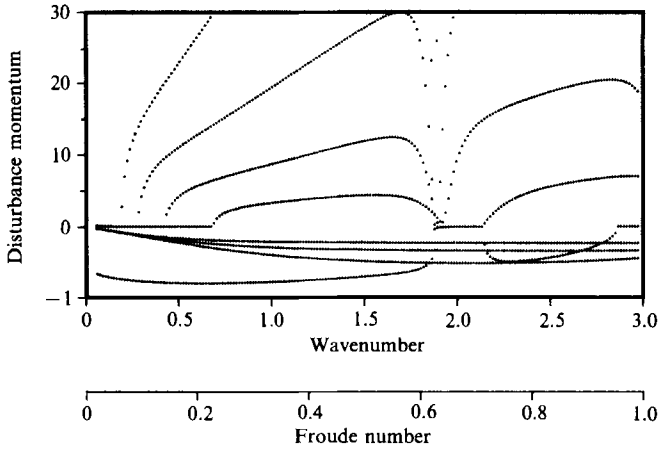

FIGURE 10. Disturbance momentum for the waves with negative phase speed. The disturbance momenta are normalized by wave amplitude ($A^2 = \langle u_1^2 + v_1^2 + u_2^2 + v_2^2 \rangle$). The scale for negative momentum is multiplied by 10.

disturbance momenta for gravity modes are negative and much smaller than Rossby modes.

9. Ageostrophic baroclinic instability

In the numerical calculation described in the previous section, baroclinically unstable modes with non-zero phase speed are observed. These modes have not been found in the quasi-geostrophic studies of the baroclinic instability. Figure 11 shows dispersion curves for Rossby waves and unstable modes in the boxed section of figure 7(*a*) but notice the difference of scale. The dispersion curves for quasi-geostrophic Rossby components (23*b*) are shown by dotted lines. The dispersion curves of stable modes are almost the same as the quasi-geostrophic wave modes (28). However, the unstable modes bifurcate to two branches when the wavenumber is sufficiently small. From figure 7(*b*), it is clear that these modes are generated by resonance between the first and second unstable modes. Two unstable modes with different growth rates resonate, resulting in two unstable modes with the same growth rate and phase speed but in opposite directions.

In the quasi-geostrophic theory of the baroclinic instability, wave components with different wavenumber cannot interact with each other ($\epsilon_{nm} = 0$ for $n \neq m$). In this ageostrophic model, however, it is possible for the first Rossby wave component in the upper layer to interact with the second Rossby wave component in the lower layer, because the wave components are not symmetric about the centre of the channel (figures 12, 13), and (19*c*) gives a non-zero interaction coefficient ϵ_{nm}. Note that the quasi-geostrophic approximations fails to obtain this bifurcation despite the fact that the modes are almost in geostrophic balance. This is because the symmetry breaking, which is responsible for a non-zero mode coupling coefficient, is of the order of the Rossby number squared.

This bifurcation occurs at the intersection point of the dispersion curves for the second Rossby components. This is due to the phase lags between wave components

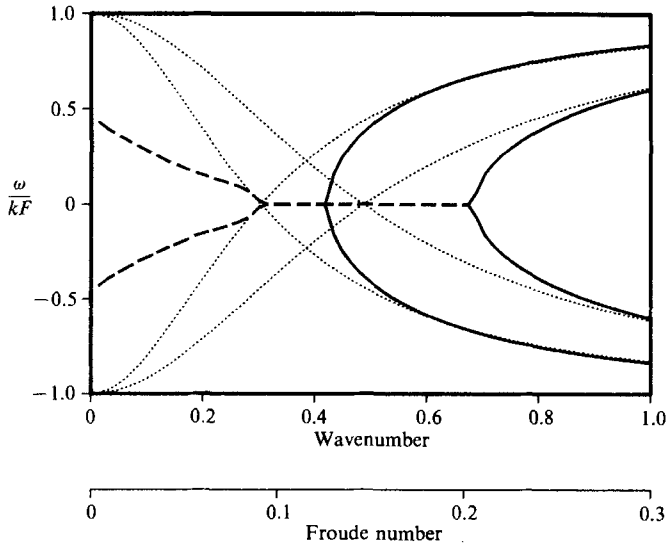

FIGURE 11. Phase speed of the lowest ageostrophic baroclinic unstable mode (thick curve). The phase speed is normalized by the non-dimensional velocity of the basic flow F. The dashed line denotes unstable modes. The dotted lines denote first and second quasi-geostrophic Rossby wave components $(\pm(\omega_n + kF)/kF)$.

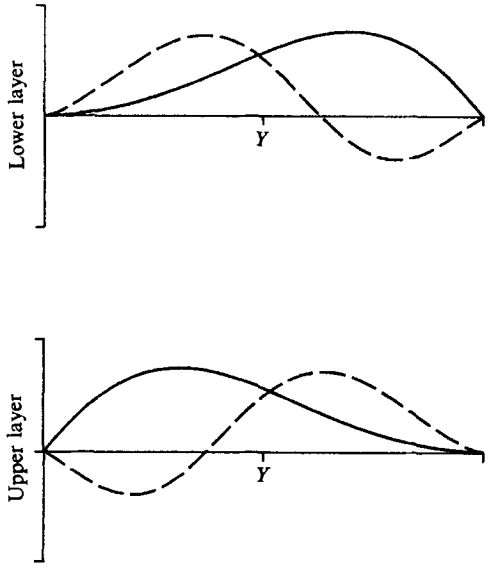

FIGURE 12. Schematic diagram of the pressure field for the first (solid lines) and second (broken lines) Rossby components. The slight asymmetry is order Rossby-number squared and is not captured by the quasi-geostrophic approximation.

in the unstable modes. From (29) the phase lag between two components in one wave model is

$$\sigma \equiv \arg\left(\frac{X_n}{Y_n}\right) \approx \arg(\tilde{\omega}_n + kU_0 + \mathrm{i}\mu), \tag{47}$$

where $\omega = \mathrm{i}\mu$ and $kU_0 \gg \mu$ is assumed. Therefore the two components in the unstable mode interact in phase ($|\sigma| < 90°$) when $\tilde{\omega}_n + kU_0 > 0$ and out of phase ($|\sigma| > 90°$)

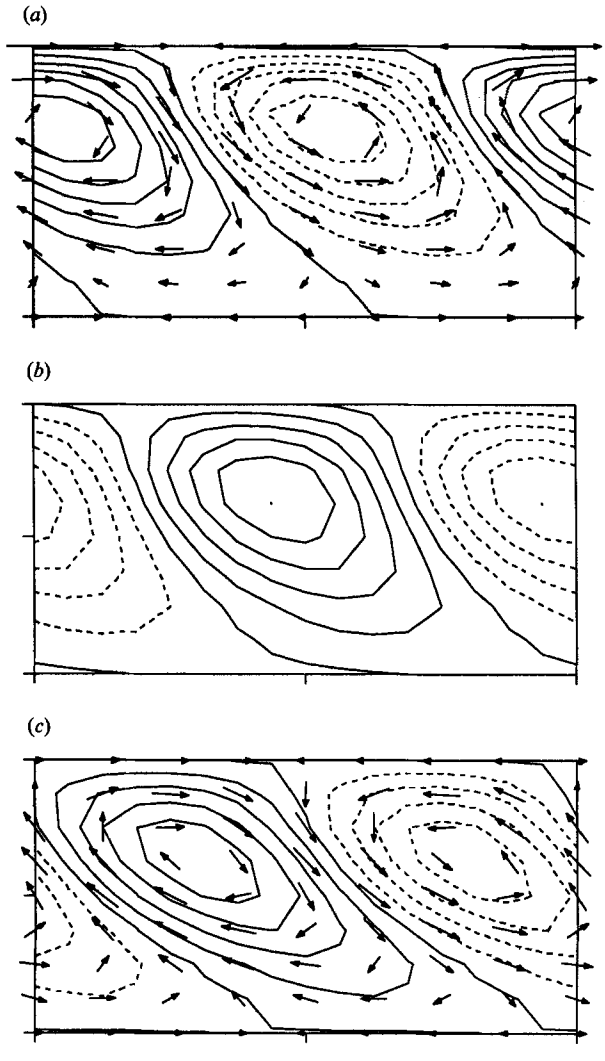

FIGURE 13. Same as figure 9, but for the ageostrophic baroclinically unstable mode ($F = 0.075$, $k = 0.225$). The contour intervals are (*a*, *c*) 0.3 and (*b*) 0.2. The geostrophic indexes are (*a*) 0.995, (*c*) 1.001.

when $\tilde{\omega}_n + kU_0 < 0$. When the second mode becomes unstable, the wave components in the first mode interact out of phase (figure 11). If the first component in the upper layer interacts with the second mode in the lower layer, the resulting second component in the upper layer is not compatible with the first component in the lower layer (figure 14*a*). Therefore resonance between unstable modes occurs only when both unstable modes have the same phase relation (figure 14*b*).

10. Discussion

Although this is the first time that the R–K instability has been discussed explicitly in terms of resonance between a Kelvin wave and Rossby waves, R–K instability seems to have been observed in several studies.

Griffiths & Linden (1982) experimentally studied a density front in a two-layer

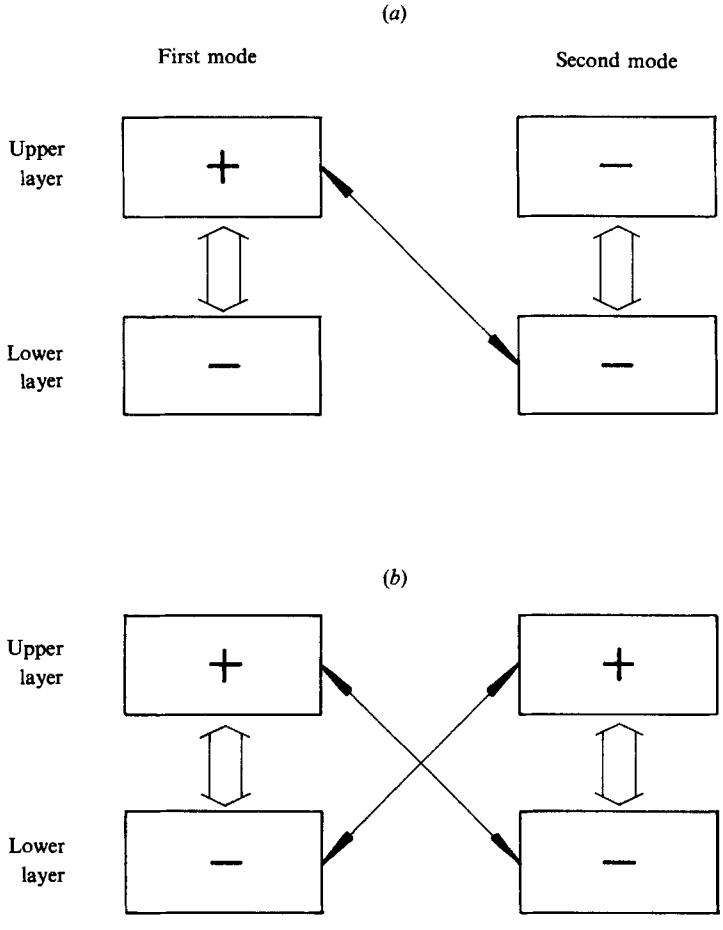

FIGURE 14. Phase relation of the wave components in the first and second baroclinic unstable modes.

system with uniform potential vorticity in the upper layer. They found that the front was unstable and the unstable mode remained almost stationary when the amplitude was small. This instability can be interpreted in the present context as follows. In their model, the basic flow in the upper layer had a velocity of $(g'H)^{\frac{1}{2}}$ relative to the lower layer at the edge of the front. Therefore the gravity wave propagating in the upstream direction can interact with a Rossby wave in the lower layer which has a very small phase speed compared with the gravity wave. The resulting unstable mode is expected to be almost stationary. Paldor (1983) showed that this frontal system was completely stable if the lower layer had infinite depth and Killworth, Paldor & Stern (1984) showed that finite depth of the lower layer destabilized the front. These two studies support the contention that the instability observed in Griffiths & Linden (1982) was an R–K instability, because the infinite depth of the lower layer results in zero potential vorticity in the lower layer and so no Rossby wave is possible.

Although Griffiths & Linden (1982) and Killworth *et al.* (1984) pointed out that Phillips' model successfully explains the wavenumber of maximum growth, it seems to be difficult to distinguish R–K instability from baroclinic instability in Phillips' model using only the wavenumber for maximum growth rate, especially when the

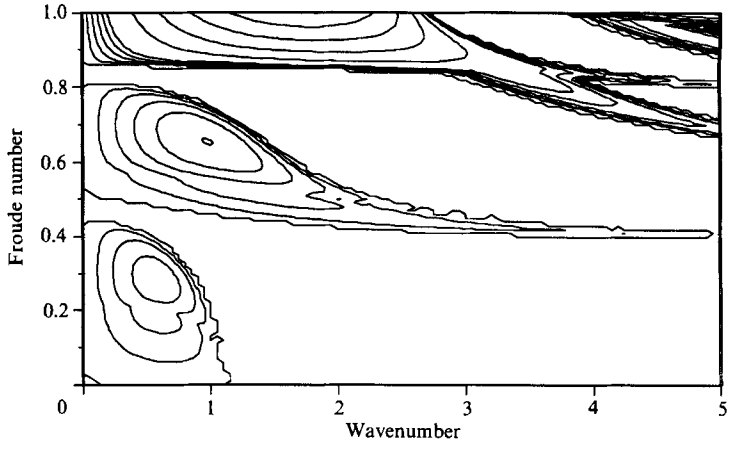

FIGURE 15. Maximum growth rate for $\Delta H = 0.8$.

Wave type	Vertical interaction	Horizontal interaction
Rossby–Rossby	Baroclinic instability (many papers)	Barotropic instability (many papers)
Rossby–gravity	R–K Instability (Griffiths & Linden 1982) (Killworth *et al.* 1984) (Stone* 1966, 1970) (Nakamura* 1988) (Present paper)	Frontal instability (one-layer model) (Killworth & Stern 1982) (Kubokawa 1985) (Young *et al.* paper in preparation)
Gravity–gravity	K–H Instability (many papers)	Instability in a shear flow with $Q = 0$ (Satomura 1981) (Kubokawa 1986) (Hayashi & Young 1987)

* Ageostrophic Eady model.

TABLE 1. Categories of instability

interface intersects the surface as in Griffiths & Linden (1982). Figure 15 shows the growth rate for a wider channel ($\Delta H = 0.8$). Comparing figure 15 with figure 6, the difference in wavenumber for maximum growth rate between an R–K instability and a baroclinic instability becomes smaller as ΔH increases.

The frontal system with a positive potential vorticity gradient towards the front in the upper layer can be unstable even if the lower layer has infinite depth (one-layer model) (Killworth & Stern 1982). This type of instability is also studied by Kubokawa (1985). It can be interpreted in the present context by resonance between a frontal trapped Kelvin wave and a Rossby wave in one layer (W. R. Young, G. R. Ierley & S. Sakai, paper in preparation). In this case, the waves interact horizontally in contrast to the vertical interaction in the R–K instability discussed above. If we distinguish this instability from the R–K instability described, we have six categories of instability defined by type of resonating wave and spatial alignment of the waves (table 1). From this table, it is clear that R–K instability should be distinguished from the so-called 'mixed instability', which usually means one due to both baroclinic and barotropic instability.

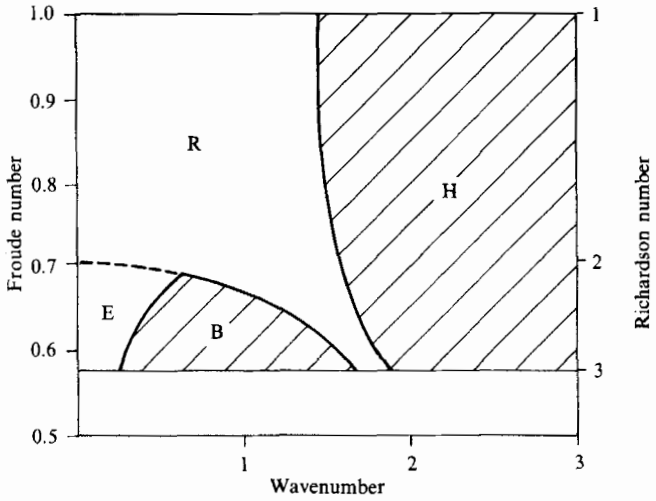

FIGURE 16. The results of Orlanski (1966) (figure 10) redrawn in the non-dimensional units of the present model. The branch R overlies the branch E. The shaded areas indicate the complex eigenvalues (non-zero phase speed).

A one-layer system with uniform potential vorticity can also be unstable when two gravity waves propagating in opposite directions resonate with each other. This type of instability has been studied by Satomura (1981), Kubokawa (1986) and Hayashi & Young (1987).

Another two-layer frontal model was studied by Orlanski (1968). In his model, the interface intersects with the surface and the bottom. He found that the front is always unstable and there are several types of instability depending on the parameter. The R–K instability should be included in these instabilities. His result (figure 10 in his paper) is redrawn in figure 16 with the present notation. Although he explained that the unstable branch R corresponds to Rayleigh instability and H corresponds to (Kelvin)–Helmholtz instability, the branch R presumably corresponds to both instabilities (K–H instability when the Richardson number (R_i) is large, and Rayleigh instability when R_i is small) because: (i) the phase speed of the lowest K–H unstable mode should be zero, but the mode H has non-zero phase speed; (ii) both instabilities are associated with the velocity shear across the interface; and (iii) the gravity effect, which stabilizes the interface and characterize the K–H instability, changes smoothly by changing the slope of the interface as the Richardson number changes. Therefore, the unstable mode R corresponds to K–H instability in the range of Froude number discussed in the present paper ($F < 1$). The K–H unstable mode R resonates with another stationary unstable mode E (baroclinic instability) and results in an unstable mode B with non-zero phase speed. This means that the unstable mode B consists of both Rossby waves and gravity waves. Furthermore, for the wider channel ($\Delta H = 0.8$) in figure 15, the branch B in Orlanski's model occupies almost the same parameter range as the R–K instability in the present model. Therefore the branch B seems to correspond to the R–K instability.

R–K-type instability is also found in a continuously stratified model (ageostrophic version of the Eady model). Stone (1966, 1970) found some unstable modes with phase speed different from that of the average basic flow (note that the conventional baroclinic instability has the same phase speed as the average basic flow). It is

identified by Nakamura (1988) as an instability due to the inertial critical layer. He showed that this unstable mode is caused by an interaction between a vorticity mode trapped at the boundary and an inertial gravity mode which has intrinsic frequency of order f and is trapped in the inertial critical layer.

Since $|M_R| \gg |M_g|$ for Rossby wave components, the Rossby–Rossby unstable mode mainly transfers momentum M_R between different places where interacting Rossby waves exist. Similarly, the gravity–gravity unstable mode transfers momentum M_g, because $|M_g| \gg |M_R|$ for gravity waves. The Rossby–gravity unstable mode induces a transfer between M_R and M_g. Therefore these six instabilities can be identified by a momentum analysis. It is difficult to identify the type of these instabilities from energy analysis because it depends on the frame of reference. The transferred disturbance momentum $(M_R + M_g)$ always has an opposite shear to that of the basic flow. In the present case, disturbance momentum in the upper layer is always negative, and that in the lower layer is always positive for unstable modes.

The R–K-type instability is also possible in the western boundary current in the ocean because the vertical difference in the mean velocity field is of the same order as the phase speed of internal gravity waves, $O(1$ m/s). If the potential vorticity is conserved along streamlines in the western boundary until the current becomes unstable and the dissipation process becomes dominant, potential vorticity in the western boundary current should be homogenized as well as the interior region. If this happens in the western boundary, it is hard to imagine that the conventional baroclinic instability initiates the meander of the current.

11. Conclusion

A criterion for instability of a two-layer model is obtained using a physical wave coordinate system. The flow is unstable if there is a pair of wave components such that (i) they are propagated in the opposite direction to the basic flow ($\tilde{\omega}_1 \tilde{\omega}_2 < 0$), (ii) they have almost the same Doppler-shifted frequency ($\tilde{\omega}_1 + kU_0 \approx \tilde{\omega}_2 - kU_0$), (iii) they can interact with each other ($\epsilon_{nm} \neq 0$). Since the wave component has disturbance momentum in the direction of the intrinsic phase speed, the disturbance momentum for the unstable mode is cancelled out by the summation of the disturbance momentum for the constituent wave components. This is consistent with the results of Hayashi & Young (1987).

A new type of instability (R–K instability) is found in an ageostrophic version of Phillips' model. The new instability is caused by resonance between a Kelvin wave and a Rossby wave, which have disturbance momenta in opposite directions. The Rossby wave is almost completely in geostrophic balance while the Kelvin wave is the same as in a one-layer system. This instability is presumably the mechanism of the frontal instability observed by Griffiths & Linden (1982) and studied by Paldor, Killworth, Stern etc. Although the present model does not include the horizontal shear in the upper layer, the results are consistent with these studies.

Including this type of instability, we have defined six categories of instabilities (table 1), according to the type of interacting wave and alignment of the waves. These instabilities can be identified by a momentum analysis. The energy analysis does not give a unique identification of the instabilities because it depends on the frame of reference. Therefore, the mechanism of the instability should be discussed in terms of disturbance momentum rather than the energy.

Ageostrophic baroclinic instability with non-zero phase speed is also found in the

numerical calculations. This instability is caused by resonance between different modes of the baroclinic instability. Although the modes involved in this instability are almost in geostrophic balance, quasi-geostrophic theory does not capture this instability. This is because it relies on a symmetry which is broken at order Rossby-number squared.

The author is grateful to Professor W. R. Young and Dr Y.-Y. Hayashi for their useful suggestions and fruitful discussion. Mr Bud Brown is acknowledged for drawing some figures. This work was carried out at the Department of Earth, Atmospheric and Planetary Sciences, MIT. The author was supported by Office of Naval Research grant no. N00014-85-G-02412.

Appendix A. Derivation of (19) from (9)

Suppose $\tilde{\omega}^*_{1n}$ is an eigenvalue of the adjoint equation (14) and $\bar{\boldsymbol{e}}_{1n}$ is the corresponding eigenvector (15), i.e.

$$\tilde{\omega}^*_{1n}\bar{\boldsymbol{e}}_{1n} - \bar{\boldsymbol{A}}_1\cdot\bar{\boldsymbol{e}}_{1n} = 0, \tag{A 1a}$$

$$\bar{\boldsymbol{e}}_{1n} \equiv (\bar{u}_{1n}, \bar{v}_{1n}, \bar{p}_{1n})^{\mathrm{T}} = \left(H_1 u_{1n}, H_1 v_{1n}, \frac{1}{g'} p_{1n}\right)^{\mathrm{T}}. \tag{A 1b}$$

Multiplying (9) by ${}^t\bar{\boldsymbol{e}}^*_{1n}$ and integrating over the channel results in

$$\hat{D}_1 \int \bar{\boldsymbol{e}}^{*\mathrm{T}}_{1n}\cdot\hat{\boldsymbol{z}}_1\,\mathrm{d}y - \int \bar{\boldsymbol{e}}^{*\mathrm{T}}_{1n}\cdot\boldsymbol{A}_1\cdot\hat{\boldsymbol{z}}_1\,\mathrm{d}y = \hat{D}_1 \int \bar{\boldsymbol{e}}^{*\mathrm{T}}_{1n}\cdot\boldsymbol{B}\cdot\hat{\boldsymbol{z}}_2\,\mathrm{d}y. \tag{A 2}$$

Using (17) and (A 1), the second term in (A 2) is reduced to

$$\int \bar{\boldsymbol{e}}^{*\mathrm{T}}_{1n}\cdot\boldsymbol{A}_1\cdot\hat{\boldsymbol{z}}_1\,\mathrm{d}y = \int (\bar{\boldsymbol{A}}_1\cdot\bar{\boldsymbol{e}}_{1n})^{*\mathrm{T}}\cdot\hat{\boldsymbol{z}}_1\,\mathrm{d}y = \tilde{\omega}_{1n} d_{1n} X_n. \tag{A 3}$$

Similarly to (18), $\hat{\boldsymbol{z}}_2$ is written as

$$\begin{aligned}\hat{\boldsymbol{z}}_2 &\equiv (\hat{u}_2(y), \hat{v}_2(y), \hat{p}_2(y))^{\mathrm{T}} \\ &= \sum_m \frac{1}{d_{2m}} Y_m \boldsymbol{e}_{sm} = \sum_m \frac{1}{d_{2m}} Y_m (u_{2m}, v_{2m}, p_{2m})^{\mathrm{T}}.\end{aligned} \tag{A 4}$$

Using (17), (A 3) and (A 4), (A 2) is reduced to

$$\hat{D}_1 X_n - \tilde{\omega}_{1n} X_n = \hat{D}_1 \sum_m \epsilon_{nm} Y_m, \tag{A 5a}$$

where

$$\epsilon_{nm} = \frac{1}{g' d_{1n} d_{2n}} \int p^*_{1n} p_{2m}\,\mathrm{d}y. \tag{A 5b}$$

In the same way, we obtain an equation for the lower layer.

The absolute value of ϵ_{nm} is limited by

$$\begin{aligned}|\epsilon_{nm}|^2 &= \frac{1}{(g' d_{1n} d_{2n})^2} \int p_{1n} p^*_{2m}\,\mathrm{d}y \int p^*_{1n} p_{2m}\,\mathrm{d}y \\ &\leqslant \left(\frac{1}{g' d^2_{1n}} \int p_{1n} p^*_{1n}\,\mathrm{d}y\right)\left(\frac{1}{g' d^2_{2n}} \int p_{2m} p^*_{2m}\,\mathrm{d}y\right) < 1,\end{aligned} \tag{A 6}$$

where the Cauchy–Schwarz inequality and (16b) are used.

Appendix B

Equation (39) can be written in the form:

$$\boldsymbol{A}\cdot\boldsymbol{x} = \omega\boldsymbol{B}\cdot\boldsymbol{x}, \tag{B 1a}$$

$$\boldsymbol{x} = (\hat{u}_1, \hat{u}_2, \hat{v}_1, \hat{v}_2, \hat{p}_1, \hat{p}_2)^{\mathrm{T}}, \tag{B 1b}$$

$$\boldsymbol{B} = \begin{pmatrix} 1 & 0 & 0 & 0 & 0 & 0 \\ 0 & 1 & 0 & 0 & 0 & 0 \\ 0 & 0 & 1 & 0 & 0 & 0 \\ 0 & 0 & 0 & 1 & 0 & 0 \\ 0 & 0 & 0 & 0 & 1 & -1 \\ 0 & 0 & 0 & 0 & 1 & -1 \end{pmatrix}. \tag{B 1c}$$

Note that the notation for $\boldsymbol{A}$, $\boldsymbol{B}$, and $\boldsymbol{x}$ is different from the text. Because eigenvalues of $\boldsymbol{B}$ contains two zero eigenvalues, we have two sets of infinite eigenvalues for the problem (B 1). These eigenvalues correspond to a barotropic pressure field (p_1+p_2), which is dependent on the other variables. Therefore we can reduce the six equations with six variables (B 1) to four equations with four variables, which contains four sets of waves (two sets of gravity waves and two sets of Rossby waves).

Eliminating $\hat{p}_j$ from equations for $\hat{u}_1$ and $\hat{u}_2$ in (38), we have

$$-\mathrm{i}\omega\zeta_1 + \mathrm{i}kF\zeta_1 + \gamma_1 = 0, \quad -\mathrm{i}\omega\zeta_2 - \mathrm{i}kF\zeta_2 + \gamma_2 = 0, \tag{B 2a, b}$$

where

$$\zeta_j = \mathrm{i}kv_j - \partial_y u_j, \quad \gamma_j = \mathrm{i}ku_j + \partial_y v_j. \tag{B 3a, b}$$

Using equations for pressure in (39), we have

$$\mathrm{i}kF(\hat{p}_2 - \hat{p}_1) = -F(\hat{v}_1 - \hat{v}_2) + (1-Fy)\gamma_1 + (1+Fy)\gamma_2, \tag{B 4a}$$

$$-\mathrm{i}\omega(\hat{p}_2 - \hat{p}_1) = -F(\hat{v}_1 + \hat{v}_2) + (1-Fy)\gamma_1 - (1+Fy)\gamma_2. \tag{B 4b}$$

Substituting equations for u_j in (39) into (B 4b), we have

$$-\mathrm{i}\omega F(\hat{u}_1 - \hat{u}_2) = (1-Fy)\gamma_1 + (1+Fy)\gamma_2 - \mathrm{i}kF^2(\hat{u}_1 + \hat{u}_2). \tag{B 5}$$

Substituting (B 4b) into (B 4a), we have

$$\begin{aligned} -\mathrm{i}\omega\{F(\hat{v}_1 - \hat{v}_2) - (1-Fy)\gamma_1 - (1+Fy)\gamma_2\} \\ = \mathrm{i}k\{F^2(\hat{v}_1 + \hat{v}_2) - F(1-Fy)\gamma_1 + F(1+Fy)\gamma_2\}. \end{aligned} \tag{B 6}$$

Substituting (B 3) into (B 2), (B 5) and (B 6), we have four first-order (in time) equations with four variables $(\hat{u}_1, \hat{u}_2, \hat{v}_1, \hat{v}_2)$. These equations are solved numerically following Hayashi & Young (1987) with boundary condition

$$\hat{v}_j = 0 \quad \text{at} \quad y = \pm Y_{\max}.$$

The y-interval is discretized by $\Delta y = Y_{\max}/N$ and the variable u_j is defined at $N+1$ points (including the points on the wall) across the channel. The variable v_j is defined at $N-1$ points excluding the boundary because v_j is fixed there. The equations are evaluated at the centre of two points for u_j and v_j (N points). To survey a wide range of the parameters, most computations were done with relatively low resolution ($N = 8$). The results were tested against a higher resolution run ($N = 16, 22$) at some parameters. In general, the computation with $N = 8$ has sufficient accuracy for lower modes.

REFERENCES

CAIRNS, R. A. 1979 The role of negative energy waves in some instabilities. *J. Fluid Mech.* **92**, 1–14.

CHARNEY, J. G. 1947 The dynamics of long waves in a baroclinic westerly current. *J. Met.* **4**, 135–163.

EADY, E. T. 1949 Long waves and cyclone waves. *Tellus* **1**, 33–52.

GRIFFITHS, R. W. & LINDEN, P. F. 1982 Laboratory experiments on fronts Part I: Density-driven boundary currents. *Geophys. Astrophys. Fluid Dyn.* **19**, 159–187.

HAYASHI, Y. & YOUNG, W. R. 1987 Stable and unstable shear modes on rotating parallel flows in shallow water. *J. Fluid Mech.* **184**, 477–504.

HIDE, R. & MASON, P. J. 1975 Sloping convection in a rotating fluid. *Adv. Phys.* **24**, 47–100.

KELVIN, LORD 1871 Hydrokinetic solutions and observations. *Phil. Mag.* **42** (4), 362–377.

KILWORTH, P. D., PALDOR, N. & STERN, M. E. 1984 Wave propagation and growth on a surface front in a two-layer geostrophic current. *J. Mar. Res.* **42**, 761–785.

KILLWORTH, P. D. & STERN, M. E. 1982 Instabilities on density-driven boundary currents and fronts. *Geophys. Astrophys. Fluid Dyn.* **22**, 1–28.

KUBOKAWA, A. 1985 Instability of a geostrophic front and its energetics. *Geophys. Astrophys. Fluid Dyn.* **33**, 223–257.

KUBOKAWA, A. 1986 Instability caused by the coalescence of two modes of a one-layer coastal current with a surface front. *J. Oceanogr. Soc. Japan* **42**, 373–380.

MECHOSO, C. R. & SINTON, D. M. 1983 On the energy analysis of the two-layer frontal model. *J. Atmos. Sci.* **40**, 2069–2074.

NAKAMURA, N. 1988 The scale selection of baroclinic instability – effect of stratification and non-geostrophy. *J. Atmos. Sci.* **45**, 3253–3267.

ORLANSKI, I. 1968 Instability of frontal waves. *J. Atmos. Sci.* **25**, 178–200.

PALDOR, N. 1983 Linear stability and stable modes of geostrophic modes. *Geophys. Astrophys. Fluid Dyn.* **24**, 299–326.

PEDLOSKY, J. 1979 *Geophysical Fluid Dynamics.* Springer.

PHILLIPS, N. A. 1954 Energy transformations and meridional circulations associated with simple baroclinic waves in a two-level, quasigeostrophic model. *Tellus* **6**, 273–286.

RIPA, P. 1983 General stability conditions for zonal flows in a one-layer model on the beta-plane of the sphere. *J. Fluid Mech.* **126**, 436–489.

SATOMURA, T. 1981 An investigation of shear instability in a shallow water. *J. Met. Soc. Japan* **59**, 148–167.

STONE, P. 1966 On non-geostrophic baroclinic stability. *J. Atmos. Sci.* **23**, 390–400.

STONE, P. 1970 On non-geostrophic baroclinic stability: Part II. *J. Atmos. Sci.* **27**, 721–726.